



## Abstract

Severe haze hovered over large areas of China in January 2013 right after the public release of  $\text{PM}_{2.5}$  data of major cities in China at the very first time. This historical severe haze emerged over the northern China with monthly average concentrations of  $\text{PM}_{2.5}$ ,  $\text{SO}_2$ , and  $\text{NO}_2$  exceeding 225, 200, and  $80 \mu\text{g m}^{-3}$ , respectively. Surface aerosol mean concentration of Beijing in January 2013 reached record high (only slightly lower than 2006) compared to historical data from 2003–2012, but with the largest daily fluctuation. Anomalous meteorological conditions in 2013 compared to the mean climatology from 2007–2012 were especially favorable for the formation of haze, such as higher humidity, lower temperature, lower PBL height, lower wind speed, and the high frequency of fog occurrences. The field campaign in Beijing showed an extremely high  $\text{PM}_{2.5}$  average concentration of  $299.2 \pm 79.1 \mu\text{g m}^{-3}$  with extremely low visibility of  $0.92 \pm 0.82 \text{ km}$  during an episode of high relative humidity with fog events. High AOD (Aerosol Optical Depth) was observed during fog days but with relatively low Angstrom exponent ( $< 1.0$ ), suggesting the modification of fog processing on the particle size. Major aerosol chemical species, such as  $\text{SO}_4^{2-}$ ,  $\text{NO}_3^-$ ,  $\text{NH}_4^+$ ,  $\text{Cl}^-$ ,  $\text{K}^+$ , and  $\text{C}_2\text{O}_4^{2-}$  presented an explicit exponential growth relationship with relative humidity, suggesting the significant impact of aerosol hygroscopicity on the visibility impairment.  $\text{SO}_4^{2-}$  increased  $\sim 5$  folds while  $\text{NO}_3^-$ ,  $\text{NH}_4^+$ , and  $\text{C}_2\text{O}_4^{2-}$  increased  $\sim 3$  folds in the fog days compared to the non-fog days. Aerosol in fog days was much more acidic than that in non-fog days. The in situ aerosol pH ranged from  $-0.78$  to  $0.14$  in fog days based on the E-AIM model simulation. Bisulfate ( $\text{HSO}_4^-$ ) accounted for 52 % of the total sulfate and free hydrogen ion ( $\text{H}_{\text{Aq}}^+$ ) accounted for 27 % of the total acids in average. Enhanced coal combustion during the winter heating season along with traffic and industrial emissions were recognized to be the major causes for this severe haze. Fog processing was found to be the major pathway of producing extremely high yields of secondary inorganic aerosol and impacting the neutralization process (i.e. aerosol acidity) in this study.

## Beijing 2013 extreme haze pollution

K. Huang et al.

Title Page

Abstract

Introduction

Conclusions

References

Tables

Figures

◀

▶

◀

▶

Back

Close

Full Screen / Esc

Printer-friendly Version

Interactive Discussion



## 1 Introduction

Haze is a weather pattern of the interaction of atmospheric water vapor with dust, smoke, and various types of particles. It is the phenomena of reduced visibility, generally, defined as less than 10 km. In the clean atmosphere, atmospheric visibility can reach about 200 km, while in the polluted atmosphere, visibility can be significantly reduced, often to just a few kilometers.

One large brown cloud has existed over the entire Indo-Asian-western Pacific region since 1990s when it was found. East Asia (including China, Thailand, Vietnam, and Cambodia) is one of the five major regional hot spots, where anthropogenic aerosol optical depth exceeded 0.3 and the absorption AOD exceeded 0.03. The Asian Brown Clouds could reduce the annual mean surface solar radiation by as large as  $10 \text{ W m}^{-2}$  or even more (Ramanathan et al., 2007). China has been maintaining an annual economic growth rate of more than 8%, which was mainly achieved through the intensive energy consumption. However, the environment in China has made concessions to the economic growth resulting in a severe air-pollution over China. The northern and eastern parts of China have become the most polluted regions with extremely high  $\text{PM}_{2.5}$  concentrations of annual values of more than  $80 \mu\text{g m}^{-3}$  based on a global map of surface  $\text{PM}_{2.5}$  concentrations approximated by incorporating a global 3-D chemical transport model with satellite data (van Donkelaar et al., 2010). Haze clouds often formed over the North China Plain with different formation mechanisms and contrasting physico-chemical properties (Tao et al., 2012). The formation of haze is closely related to the meteorological conditions and the concentration of atmospheric pollutants (Chow et al., 2002; Zhao et al., 2013). Aircraft measurement in North China revealed that the highly efficient coating of dust particles by pollution acids could provide predominant source of cloud condensation nuclei, forming widespread haze – clouds over China (Ma et al., 2010). The cost to health of residents caused by air pollution in Beijing was estimated to account for 6.55% of its GDP (gross domestic product) (Zhang et al., 2007a).

Title Page

Abstract

Introduction

Conclusions

References

Tables

Figures

◀

▶

◀

▶

Back

Close

Full Screen / Esc

Printer-friendly Version

Interactive Discussion



**Beijing 2013 extreme haze pollution**

K. Huang et al.

Title Page

Abstract

Introduction

Conclusions

References

Tables

Figures

◀

▶

◀

▶

Back

Close

Full Screen / Esc

Printer-friendly Version

Interactive Discussion



During January 2013, an unprecedented air pollution shrouded over the northeastern China. The hourly  $PM_{2.5}$  levels in many cities were even off-the-scale beyond the upper limits of the Air Quality Index (Wong, 2013). In Beijing, many residents rushed to buy face masks and air purifiers. The number of patients with respiratory problems had increased sharply during this period, while many airports were shut down and most of the flights were canceled due to the extremely low visibility (<http://www.theguardian.com/world/2013/feb/16/chinese-struggle-through-airpocalypse-smog>). Since China released its nationwide  $PM_{2.5}$  observation data from 1 January 2013 at the first time, this unprecedented air pollution right after this act had attracted tremendous attentions from both domestic and abroad. Various media had reported this breaking news and China's air pollution issues have been raised to a nationwide attention. Zhang et al. (2014) compared the meteorology over East China in January 2013 with historical data using the NCEP reanalysis products. Anomalous meteorology was found for this persistent severe fog and haze, explaining about 2/3 of the variance of daily visibility evolution. In Beijing, the Plam index (based on wind speed/direction, relative humidity, temperature, evaporability, and stability) reached very high values, far exceeding those in the relative clean days (Zhang et al., 2013a). Within the framework of the CARE-China network, Wang et al. (2014a) identified this widespread haze pollution in the Beijing-Tianjing-Heibei area. The unusual atmospheric circulation was found very unfavorable for the cleanup of the air pollution and two stages of aerosol growth were revealed, i.e. the “explosive growth” and “sustained growth”. Zhang et al. (2013b) reported the chemical composition and conducted source apportionment of  $PM_1$  in Beijing during January 2013 using an Aerodyne High-Resolution Time-of-Flight Aerosol Mass Spectrometer (AMS). Model simulation indicated that regional transport played an important role in the formation of regional haze over the Beijing-Tianjin-Heibei area (Wang et al., 2014b, 2013), and consideration of the two-way feedback between meteorology and atmospheric chemistry could greatly improve the model performance and this effect contributed as large as 30 % of the monthly average  $PM_{2.5}$  concentrations (Wang et al., 2014b).

**Beijing 2013 extreme haze pollution**

K. Huang et al.

[Title Page](#)[Abstract](#)[Introduction](#)[Conclusions](#)[References](#)[Tables](#)[Figures](#)[◀](#)[▶](#)[◀](#)[▶](#)[Back](#)[Close](#)[Full Screen / Esc](#)[Printer-friendly Version](#)[Interactive Discussion](#)

In this study, the anomalous meteorological conditions were examined by using nationwide ground-based meteorology data in January 2013, different from previous study using the reanalysis data. A special attention was paid to the high frequency of fog days accompanied with high relative humidity. The formation mechanism of this extremely severe haze in regard of aerosol chemistry was explicitly illustrated based on the field measurement during the first half of January 2013. Especially, the role of fog processing in contributing to the high yields of secondary aerosol formation was revealed. The aqueous-phase processing was found to be a major pathway of determining the neutralization process, aerosol acidity and existence form of acidic species.

## 2 Methodology

### 2.1 Observation site and field sampling

The observation site in Beijing was set up on the roof of a 20 m-tall teaching building on campus of Beijing University of Technology. It is located between the 3rd and 4th ring roads of Beijing. This site is situated in an area of mixed emissions such as residential, traffic, construction, and industrial sources. PM<sub>2.5</sub> aerosol samples were collected on Whatman<sup>®</sup> 41 filters (Whatman Inc., Maidstone, UK) using medium-volume samplers manufactured by Beijing Geological Instrument-Dickel Co., Ltd. (model: TSP/PM<sub>10</sub>/PM<sub>2.5</sub>-2; flow rate: 77.59 Lmin<sup>-1</sup>). The duration time of sampling was generally 24 h. The filters before and after sampling were weighed using an analytical balance (Model: Sartorius 2004MP) with a reading precision 10 µg after stabilizing in constant temperature (20 ± 1°C) and humidity (40% ± 1%) for 48 h. All the procedures were strictly quality controlled to avoid the possible contamination of samples.

## 2.2 Chemical analysis

### 2.2.1 Ion analysis

One-fourth of each sample and blank filter was extracted ultrasonically by 10 mL deionized water ( $18\text{ M}\Omega\text{ cm}^{-1}$ ). Eleven inorganic ions ( $\text{SO}_4^{2-}$ ,  $\text{NO}_3^-$ ,  $\text{F}^-$ ,  $\text{Cl}^-$ ,  $\text{NO}_2^-$ ,  $\text{PO}_4^{3-}$ ,  $\text{NH}_4^+$ ,  $\text{Na}^+$ ,  $\text{K}^+$ ,  $\text{Ca}^{2+}$ ,  $\text{Mg}^{2+}$ ) and four organic acids (formic, acetic, oxalic, and methylsulfonic acid, MSA) were analyzed by Ion Chromatography (ICS 3000, Dionex), which consisted of a separation column (Dionex Ionpac AS 11), a guard column (Dionex Ionpac AG 11), a self-regenerating suppressed conductivity detector (Dionex Ionpac ED50) and a gradient pump (Dionex Ionpac GP50). The detail procedures were given elsewhere (Yuan et al., 2003).

### 2.2.2 Element analysis

Half of each sample and blank filter was digested at  $170^\circ\text{C}$  for 4 h in high-pressure Teflon digestion vessel with 3 mL concentrated  $\text{HNO}_3$ , 1 mL concentrated  $\text{HClO}_4$ , and 1 mL concentrated HF. After cooling, the solutions were dried, and then diluted to 10 mL with distilled deionized water. Total 24 elements (Al, Fe, Mn, Mg, Mo, Ti, Sc, Na, Ba, Sr, Sb, Ca, Co, Ni, Cu, Ge, Pb, P, K, Zn, Cd, V, S, and As) were measured by using an inductively coupled plasma atomic emission spectroscopy (ICP-OES; SPECTRO, Germany). The detailed analytical procedures were given elsewhere (Zhuang et al., 2001).

## 2.3 Supplementary datasets

### 2.3.1 Meteorology data

The meteorology and visibility data over the whole China used in this study is from the Global Summary of Day (GSOD) database distributed by the US National Climatic Data Center (NCDC). Over 8000 stations' data in the whole world are available and

Title Page

Abstract

Introduction

Conclusions

References

Tables

Figures

◀

▶

◀

▶

Back

Close

Full Screen / Esc

Printer-friendly Version

Interactive Discussion



are made accessible through <http://www.ncdc.noaa.gov/>. A total of 12 surface meteorological parameters derived from the hourly observations are available in the GSOD database. Also, information about the occurrence of fog, rain, snow, hail, thunder, and tornado/funnel clouds are included. An extensive automated quality control was applied to correctly “decode” as much of the synoptic data as possible and to eliminate random errors found in the original data (Lott, 2004; Smith et al., 2011).

### 2.3.2 China API and AQI data

Before 2013, API (Air Pollution Index) was the official data released by the Ministry of Environment Protection of China (MEP) (<http://datacenter.mep.gov.cn/>) for routinely reporting the air quality. The calculation of API was based on five air pollutants, i.e. SO<sub>2</sub>, NO<sub>2</sub>, PM<sub>10</sub>, CO, and O<sub>3</sub>, and was reported on a daily basis. Note that PM<sub>2.5</sub> was not included as part of API. Each pollutant was assigned an individual score according to their concentrations and the final API reported was as the highest of those 5 scores. API could be converted to the mass concentrations using the following formula:

$$C = C_{\text{low}} + [(I - I_{\text{low}})/(I_{\text{high}} - I_{\text{low}})] \times (C_{\text{high}} - C_{\text{low}}),$$

where  $C$  is the concentration and  $I$  is the API value.  $I_{\text{high}}$  and  $I_{\text{low}}$ , the two values most approaching to value  $I$  in the API grading limited value table, stand for the value higher and lower one than  $I$ , respectively;  $C_{\text{high}}$  and  $C_{\text{low}}$  represent the concentrations corresponding to  $I_{\text{high}}$  and  $I_{\text{low}}$ , respectively. The values in different grades could be found in (Qu et al., 2010). In this study, the historical data of particulate matter (PM<sub>10</sub>) in Beijing were derived from API.

In February 2012, MEP released the official (trial) revisions to its air quality standards and made AQI (Air Quality Index) as the standard of air pollution level, which was a notable shift from its previous form as API. Specially, PM<sub>2.5</sub> was included as part of AQI at this first time. As of 1 January 2013, MEP started to release data of six air pollutants (SO<sub>2</sub>, NO<sub>2</sub>, PM<sub>10</sub>, PM<sub>2.5</sub>, CO, and O<sub>3</sub>) at 74 cities of China. The real time database is publicly accessible via <http://113.108.142.147:20035/emcpublish/>.

Title Page

Abstract

Introduction

Conclusions

References

Tables

Figures

◀

▶

◀

▶

Back

Close

Full Screen / Esc

Printer-friendly Version

Interactive Discussion



### 2.3.3 AERONET

Aerosol optical properties in Beijing were retrieved from the Aerosol Robotic Network (AERONET, <http://aeronet.gsfc.nasa.gov/>) performed by a Cimel CE-318 sun photometer (Holben et al., 1998). The bandwidth of each channel is 10 nm. Various parameters of aerosol optical properties were retrieved at 440 nm, 670 nm, 870 nm, and 1020 nm. Aerosol size distribution, refractive index, and single-scattering albedo can be retrieved by using sky radiance almucantar measurements and direct sun measurements (Dubovik and King, 2000). The level 2.0 cloud-screened data with quality-assured were used in this study.

### 2.4 E-AIM model

The Extended Aerosol Thermodynamics Model (E-AIM) is an online tool (<http://www.aim.env.uea.ac.uk/aim/aim.php>) for calculating gas/liquid/solid partitioning in aerosol systems. The latest version is Model IV which considers a  $\text{H}^+$ - $\text{NH}_4^+$ - $\text{Na}^+$ - $\text{SO}_4^{2-}$ - $\text{NO}_3^-$ - $\text{Cl}^-$ - $\text{H}_2\text{O}$  system and allows variable temperature. Details of the model are given elsewhere (Clegg et al., 1998; Friese and Ebel, 2010). This model depends on the presence of an aqueous phase in thermodynamic equilibrium. If the ambient relative humidity (RH) is higher than the deliquescence RH of the solid phase, the particles are assumed to exist in the aqueous solution. If RH is lower than the deliquescence RH, particles will crystallize without any liquid water content. To run the E-AIM model, the molar concentrations of  $\text{SO}_4^{2-}$ ,  $\text{NO}_3^-$ ,  $\text{Cl}^-$ ,  $\text{NH}_4^+$ ,  $\text{Na}^+$ , and  $\text{H}^+$  as well as temperature and relative humidity are required. Of all the required inputs, only  $\text{H}^+$  in aerosol ( $\text{H}_{\text{Aer}}^+$ ) is not directly measured. Usually, the concentration of  $\text{H}_{\text{Aer}}^+$  is estimated using the ionic charge balance, i.e. the difference between the equivalent concentrations of the total cations and the total anions. There were different methods for estimating  $\text{H}_{\text{Aer}}^+$  in previous studies. Zhang et al. (2007b) estimated  $\text{H}_{\text{Aer}}^+$  in Pittsburg by considering a simple system:  $\text{SO}_4^{2-}$ ,  $\text{NO}_3^-$ ,  $\text{Cl}^-$ , and  $\text{NH}_4^+$ . In an early study of Hong Kong (Pathak et al., 2004,

Title Page

Abstract

Introduction

Conclusions

References

Tables

Figures

◀

▶

◀

▶

Back

Close

Full Screen / Esc

Printer-friendly Version

Interactive Discussion



Beijing 2013 extreme  
haze pollution

K. Huang et al.

Title Page

Abstract

Introduction

Conclusions

References

Tables

Figures

◀

▶

◀

▶

Back

Close

Full Screen / Esc

Printer-friendly Version

Interactive Discussion



2003),  $K^+$  and  $Ca^{2+}$  were not considered for the ionic charge balance, while  $K^+$  was considered in a more recent study in Hong Kong (Xue et al., 2011). Different from the above studies, in which those mineral ions only contributed a minor fraction in the total water soluble ions, aerosol over Beijing was frequently influenced by the mineral dust originated from the arid and semi-arid regions, such as Inner-Mongolia and the Loess Plateau (Wang et al., 2005; Huang et al., 2010a, b). Thus, it is not proper to exclude those mineral ions from the calculation of ionic balance for cities in northern China. In this study,  $H_{Aer}^+$  could be overestimated 3–72 % without accounting  $Ca^{2+}$  and  $Mg^{2+}$ . Hence,  $H_{Aer}^+$  is calculated by using the following equation as the input for the E-AIM model:  $[H_{Aer}^+] = 2[SO_4^{2-}] + [NO_3^-] + [Cl^-] - [NH_4^+] - [Na^+] - [K^+] - 2[Ca^{2+}] - 2[Mg^{2+}]$ , the units of all ions are in molar concentrations ( $\mu\text{mol m}^{-3}$ ). The ratio ( $R_{H^+}$ ) of  $H_{Aer}^+$  in the “real” total ions could be calculated as follows:

$$R_{H^+} = \begin{cases} H_{Aer}^+ / (2 \times [\text{Anions}]_{\text{total}}), & \text{if } [\text{Anions}]_{\text{total}} > [\text{Cations}]_{\text{total}} \\ 0, & \text{if } [\text{Anions}]_{\text{total}} \leq [\text{Cations}]_{\text{total}} \end{cases}$$

$\text{pH}_{\text{is}}$  is defined as the in situ pH value of the aqueous phase in aerosols and calculated by using the following equation (Xue et al., 2011; Li et al., 2013):

$$\text{pH}_{\text{is}} = -\log(\gamma_{H^+} \times n_{H^+} \times 1000 / V_a),$$

where  $\gamma_{H^+}$  represents the activity coefficient of aqueous  $H^+$ ;  $n_{H^+}$  represents the concentration of free  $H^+$  in the unit of  $\text{mol m}^{-3}$ ; and  $V_a$  is the total volume of the aqueous phase of aerosol in the unit of  $\text{cm}^3 \text{m}^{-3}$ .  $\gamma_{H^+}$ ,  $n_{H^+}$ , and  $V_a$  are all derived from the E-AIM model.

### 3 Results and discussion

#### 3.1 A historical pollution event of January 2013 over Beijing

Figure 1 shows the average values of AOD (Aerosol Optical Depth) and surface PM<sub>10</sub> concentrations over Beijing in each year's January from 2003 to 2013. Level 2.0 AOD and PM<sub>10</sub> data are retrieved from AERONET (AERosol RObotic NETwork) and the Ministry of Environment Protection of China, respectively. These two parameters showed consistent variation trends of each January during multi-years from 2003 to 2013 with the first peak shown in January 2006. The year 2006 was a turning point of China's air pollutant emissions. China's SO<sub>2</sub> emissions from various inventories all showed evident increasing trends from 2000 to 2006 (Itahashi et al., 2012). Consistently, an increasing trend of AOD from both observation and simulation was also found during this period (Itahashi et al., 2012). After 2006, obvious decreasing trends of both AOD and PM<sub>10</sub> in Beijing were observed till 2011 as shown in Fig. 1. On one hand, this period endured the implementation of China's 11th Five-Year-Plan, which specifically focused on the abatement of air pollutant emissions such as airborne particles and SO<sub>2</sub>. On the other hand, the 2008 Beijing Olympic Games evoked an excellent opportunity for Beijing and neighboring provinces (e.g. Hebei, Tianjin, and Shandong) to control their local emissions (Gao et al., 2011). Hence, the annual decreasing rate of AOD and PM<sub>10</sub> in Beijing reach 0.19 yr<sup>-1</sup> and 23.6 μg m<sup>-3</sup> yr<sup>-1</sup> during 2006–2011, respectively. However, in the recent 2 yr (2012–2013), aerosol concentrations tended to significantly rebound. Compared to the January of 2011, AOD increased 0.16 and 0.43 in 2012 and 2013, respectively. For PM<sub>10</sub>, it increased 63 and 134 μg m<sup>-3</sup>, respectively. The average surface PM<sub>10</sub> level in the January of 2013 was comparable to that of 2006, when the SO<sub>2</sub> emission of China was the highest in the last decade (Lu et al., 2010). Specifically, the range of PM<sub>10</sub> variation (shaded areas in Fig. 1a) in 2013 was the largest, about 1.3 folds of that in 2006 and 1.5–4.3 folds of the other years. This indicated that more extreme events occurred in 2013. However, the average AOD in the January of 2013

## Beijing 2013 extreme haze pollution

K. Huang et al.

Title Page

Abstract

Introduction

Conclusions

References

Tables

Figures

◀

▶

◀

▶

Back

Close

Full Screen / Esc

Printer-friendly Version

Interactive Discussion



**Beijing 2013 extreme  
haze pollution**

K. Huang et al.

Title Page

Abstract

Introduction

Conclusions

References

Tables

Figures

◀

▶

◀

▶

Back

Close

Full Screen / Esc

Printer-friendly Version

Interactive Discussion



was  $\sim 40\%$  lower than that of 2006. AOD is a measure of column particle loadings and less impacted by the height of planetary boundary layer (PBL), thus a better indicator of emission than surface concentration. This meant that even more intense emissions of air pollutants had ever occurred in Beijing before, while the 2013 January heavy pollution was actually the second intense in Beijing's history based on the available long-term measurement data. However, the 2013 haze gained much more wide attentions from both domestic and abroad due to that China made its  $\text{PM}_{2.5}$  data (along with some other air pollutants) public at the first time since the beginning of 2013. The “inconsistence” between surface particle concentration and AOD in 2013 probably indicated that other factors such as meteorological conditions played an important role in altering the relationship between surface and column loadings.

Figure 2 illustrates how severe the air pollution had emerged in northeastern China during this study period. The spatial distributions of the mean concentrations of  $\text{PM}_{2.5}$ ,  $\text{SO}_2$ , and  $\text{NO}_2$  in January 2013 at 74 Chinese cities are plotted. Figure 2a illustrates the highest concentrations of  $\text{PM}_{2.5}$  over the Beijing-Tianjin-Hebei region (highlighted by the black rectangle in Fig. 2a) with monthly average of more than  $225\ \mu\text{g m}^{-3}$ . It was reported that the hourly  $\text{PM}_{2.5}$  concentrations even reached about  $900\ \mu\text{g m}^{-3}$  during some episodes (Clean-Air-Asia, 2013). This off-the-charts level of  $\text{PM}_{2.5}$  could be considered as “crazy bad” and an air quality disaster for human health. Although Eastern China encountered lighter  $\text{PM}_{2.5}$  pollutions in this period, however, most cities located in this area still reached monthly mean  $\text{PM}_{2.5}$  concentrations of up to  $150\ \mu\text{g m}^{-3}$ . The spatial distribution of  $\text{SO}_2$  (Fig. 2b) was as similar as that of  $\text{PM}_{2.5}$  to a certain degree. However, the high-low zones of  $\text{SO}_2$  were more distinguished than  $\text{PM}_{2.5}$  and well separated by the heating supply line indicated by the dashed line in Fig. 2b. In northern China, the heating period lasted for the whole winter, resulting in enhanced coal consumption from thermal power plants and residential usage, while there were almost no heating facilities in southern China. Thus, this could explain the extremely high  $\text{SO}_2$  concentrations of more than  $200\ \mu\text{g m}^{-3}$  around the Beijing-Tianjin-Hebei region. As for  $\text{NO}_2$  (Fig. 2c), its high concentrations were not only observed in northern China but



**Beijing 2013 extreme haze pollution**

K. Huang et al.

Title Page

Abstract

Introduction

Conclusions

References

Tables

Figures

I◀

▶I

◀

▶

Back

Close

Full Screen / Esc

Printer-friendly Version

Interactive Discussion



low over mainland China while an abnormal high from the ocean to the coast. Weakening of wind velocity occurred at all levels of the troposphere (Zhang et al., 2014). Hence, this synoptic stagnation should slow down the air convection and aggravate the air pollution. The variations of temperature showed distinct behaviors dependent on regions. Northern China (mainly Inner Mongolia), northwestern China, and southern China all showed increased temperature compared to the previous years, while the major regions of northeastern China showed decreased temperature of about 1 °C, which could result in contrasting impacts on the air pollution. The lower temperature did not favor the atmospheric processing on one hand, while it favored the partitioning of ammonium salts and semi-volatile species into the particulate phase on the other hand. Also, the lower temperature could induce the formation of temperature inversion layer due to less solar heat reaching the ground. As a result, the regions where showed temperature decreases also corresponded to the decreases of PBLH as shown in Fig. 3d. It was found that the temperature anomaly increased with height below 850 hPa, causing strong anomalous inversion (Zhang et al., 2014). PBLH of the North China Plain had a significant decrease of 100–200 m, which accounted for about 40 % of the average PBLH in previous years. This dramatic decrease of PBLH would surely slow down the atmospheric convection and exacerbate the air pollution especially at the surface level. Figure 3e and f shows the number of fog days and the total amount of precipitation during January 2013, respectively. The information of fog occurrence was obtained from the NCDC ground-based meteorology observations. Considerable precipitation mainly occurred below 35° N, covering most areas of southern China, while in the other regions the monthly total precipitation amounts were less than 5 mm. The negligible wet scavenging process in the North China Plain could be another possible factor contributing to the extreme pollution. The spatial distribution of fog days generally was as similar as that of precipitation. It should be noted that a considerable number of fog days was observed in the North China Plain. The number of fog days around the Beijing-Tianjin-Hebei area reached 10–20 days in the whole month of January 2013. Winter is the season when fog easily forms. As stated above, the relative humidity over the North



### 3.3 Severe air pollution of a typical megacity in northern China

#### 3.3.1 Time series of aerosol concentration, AOD and meteorology

A half-month field measurement was conducted in Beijing, the capital city of China located in the North China Plain. Figure 4b shows the daily concentrations of PM<sub>2.5</sub> from filter sampling and AOD (500 nm) with Angstrom exponent (470–880 nm) from the Beijing AERONET site during 1–15 January 2013. The major meteorological parameters are shown in Fig. 4a. January 1–3 were the cleanest days during the whole study period with PM<sub>2.5</sub> concentration of  $36.1 \pm 2.67 \mu\text{g m}^{-3}$  in average and visibility of up to 11.8 km at most times (note that threshold of visibility reported from the weather station was 11.8 km). It was found that the winds during this period dominantly came from the northwest with high speeds of  $5.7 \pm 2.9 \text{ m s}^{-1}$ . At the same time, relative humidity stayed at low values of  $(26.6 \pm 16.3) \%$  without normal diurnal cycles as compared to the other days, i.e. lower RH around noon and higher RH during night. This clearly indicated a cold front induced by the Siberian high pressure system with air masses typically cold, dry, and relatively clean. After the cold front passed, wind speed obviously slowed down and the relative humidity returned back to a normal diurnal cycle. Daily PM<sub>2.5</sub> concentrations started to climb up and exceeded over  $100 \mu\text{g m}^{-3}$  on 6 and 7 January. Afterwards, PM<sub>2.5</sub> concentrations decreased on the following two days and a similar cold front occurred but with a shorter duration than the first one. Following this relatively clean episode, a consecutive four days severe pollution episode lasted from 10–13 January with the average PM<sub>2.5</sub> concentration of as high as  $299.2 \pm 79.1 \mu\text{g m}^{-3}$  and extremely low visibility of  $0.92 \pm 0.82 \text{ km}$ . Relatively low wind speeds ( $\sim 1.7 \text{ m s}^{-1}$ ) should be partly responsible for this as shown in Fig. 4a. Also, it was found a low pressure field dominated during this period with the formation of inversion layer (Wang et al., 2014a). The vertical difference of pseudo-equivalent potential temperature between 850 and 1000 hPa showed low values during this period (Zhang et al., 2014). Especially, it was noted that fog occurred every day since January 10 and lasted five days

Beijing 2013 extreme  
haze pollution

K. Huang et al.

Title Page

Abstract

Introduction

Conclusions

References

Tables

Figures

◀

▶

◀

▶

Back

Close

Full Screen / Esc

Printer-friendly Version

Interactive Discussion



as shown in Fig. 4. The duration of each fog episode lasted about 15 to 24 h. The low wind speeds helped to develop these long lasting fog events. Correspondingly, relative humidity reached the highest values of  $(77.7 \pm 13.4)\%$  during the whole study period. This high RH level with frequent fog occurrences should exert great impacts on the aerosol formation, which could partly explain the extremely impaired visibility shown in Fig. 4a. The measurement of aerosol optical properties from AERONET could possibly shed some light on the impact from high RH. As shown in Fig. 4b, from 6–10 January, AOD varied in a relatively consistent way with surface  $\text{PM}_{2.5}$ . The ratio of AOD vs.  $\text{PM}_{2.5}$  ranged from 2 to  $4 \text{ mg}^{-1} \text{ m}^{-3}$ . On 11 and 14 January, when fog events occurred, the ratios of  $\text{AOD}/\text{PM}_{2.5}$  were much more elevated to around 6 and  $8 \text{ mg}^{-1} \text{ m}^{-3}$ , respectively. PBL height was an important parameter impacting on the surface particle concentration and hence on the  $\text{AOD}/\text{PM}_{2.5}$  ratio. During 6–10 January, the PBL height averaged  $155.8 \pm 73.7 \text{ m}$ , compared to its values of 121.8 and 189.9 m on 11 and 14 January, respectively. The  $\pm 20\%$  difference of PBL height between the two fog days and the non-fog days probably couldn't explain the 1.5–4 folds difference of the  $\text{AOD}/\text{PM}_{2.5}$  ratios. By assuming that the extinction efficiency of  $\text{PM}_{2.5}$  varied little in a short period, this big discrepancy of the  $\text{AOD}/\text{PM}_{2.5}$  ratios between the non-fog days and fog episodes should be mainly caused by the hygroscopic growth factor, which determined the variability of aerosol extinction coefficient caused by the relative humidity. Since the hygroscopic growth factor generally increases exponentially with the increase of relative humidity, the  $\text{AOD}/\text{PM}_{2.5}$  ratios during fog events were expected to be much higher than those days with lower humidity. In addition, distinct difference of the Angstrom exponent between the fog days and non-fog days was also found. During 6–10 January (except 8 January, when it was influenced by a cold front and the mineral aerosol contributed 42 % to  $\text{PM}_{2.5}$  mass, see Supplement Fig. S2a), the Angstrom exponents stayed within 1.3–1.4, indicating the dominance of fine particles. However, during the fog days (e.g. 11, 12 and 14 January), the Angstrom exponents were all below 1.0 and this should be generally caused by a significant contribution of coarse particles. However, there were no dust events observed based on the meteorological

Beijing 2013 extreme  
haze pollution

K. Huang et al.

Title Page

Abstract

Introduction

Conclusions

References

Tables

Figures

◀

▶

◀

▶

Back

Close

Full Screen / Esc

Printer-friendly Version

Interactive Discussion



conditions (e.g. high humidity and low wind speed) and the low concentrations of mineral elements (Fig. S2a). Thus, a reasonable explanation of this phenomenon should be due to the effect of high humidity on the growth of particles. Fog was likely to dramatically increase the sizes of the particles due to the adsorption of water on the particle surface. Hence, the Angstrom exponents were found to be greatly reduced even fine particles dominated. This was consistent with the results from Li et al. (2014) based on a ground-based CIMEL sun-sky radiometer in Beijing during a similar study period. The residue aerosol mode (peaked around 0.4–0.5  $\mu\text{m}$ ) evidently increased under the influences of clouds and fog with the peak size distribution shifting to larger sizes. A typical phenomenon of fine particle coagulation was observed with the increase of volume size but with the decrease of particle numbers. Another study at various locations based on AERONET observation also showed the modification effect of fog and cloud on aerosol (Eck et al., 2012). For instance, at Kanpur, India when there was low cloud or fog nearby, a cluster of outliers would show up with high fine mode fraction of AOD ( $> 0.90$  at 440 nm) but with relatively low values of Angstrom exponent ( $< 1.0$ ). The aerosol size distribution at various sites (e.g. Kanpur, India; Arica, Chile; Fresno, California; Sao Paulo, Brazil) all showed similar bimodal submicron patterns that a stronger contribution of the larger mode ( $\sim 0.45 \mu\text{m}$ ) to AOD was found before the dissipation of fog or clouds. In this study, each fog episode lasted long durations without quick dissipations. Thus, aerosol was probably saturated by gaining sufficient water content, resulting in the relative low values of Angstrom exponent.

### 3.3.2 Chemical characterization of aerosols

The chemical speciation of aerosol further aided to reveal the characteristics of this severe haze pollution. Figure 5 shows the temporal variation of inorganic species in  $\text{PM}_{2.5}$  and the mass ratios of the total water soluble inorganic ions (TWSII) in  $\text{PM}_{2.5}$ . Generally, the temporal variation of TWSII resembled that of  $\text{PM}_{2.5}$  concentration (Fig. 4b). Except for those days impacted by cold fronts (1–3 and 8 January), the ratios of TWSII/ $\text{PM}_{2.5}$  stayed at fairly stable values of  $(40.8 \pm 2.0)\%$ . One comparable study on measurement

Beijing 2013 extreme  
haze pollution

K. Huang et al.

Title Page

Abstract

Introduction

Conclusions

References

Tables

Figures

◀

▶

◀

▶

Back

Close

Full Screen / Esc

Printer-friendly Version

Interactive Discussion



of non-refractory  $PM_{1.0}$  species by using AMS calculated the sum of sulfate, nitrate, ammonium and chloride accounted for 50.2% of  $PM_{1.0}$  (Zhang et al., 2013). It should be noted that aerosol species measured by AMS did not include refractory species such as  $Ca^{2+}$ ,  $Mg^{2+}$ ,  $Na^+$ , etc. Also, Zhang et al. (2013) measured smaller size ( $PM_{1.0}$ ) than this study ( $PM_{2.5}$ ). Thus, our results from the offline filter sampling were relatively consistent with the online measurement. Among the ions,  $SO_4^{2-}$  ( $22.4 \pm 23.5 \mu g m^{-3}$ ),  $NO_3^-$  ( $15.6 \pm 13.6 \mu g m^{-3}$ ), and  $NH_4^+$  ( $8.5 \pm 6.4 \mu g m^{-3}$ ) were the three biggest contributors, accounting for about 80% of the total ions. Zhang et al. (2013) observed very similar size distribution of sulfate, nitrate, and ammonium, suggesting their similar gas-to-particle processes. Different from the haze observed during autumn and spring in Beijing that the mass ratio of  $NO_3^-/SO_4^{2-}$  was larger than 1.0 (Sun et al., 2013b), the ratio of  $NO_3^-/SO_4^{2-}$  was around 0.7 in this study, which was very close to a study of the similar study period (Wang et al., 2014a). Enhanced coal consumption for heating should be mainly responsible for the relatively low value of this ratio.  $Cl^-$  ranked as the fourth abundant ion with the average concentration of  $4.8 \pm 3.7 \mu g m^{-3}$ . This was close to the average  $Cl^-$  level in Beijing during winter from 2001 to 2003 (Wang et al., 2005) and that during early December 2004 (Sun et al., 2006). Again, coal combustion during the heating season should be the major cause for this high level  $Cl^-$ . Other ions, e.g.  $K^+$ ,  $Na^+$ ,  $Ca^{2+}$ ,  $Mg^{2+}$ , and  $F^-$ , contributed relatively small fractions. The major secondary ions ( $SO_4^{2-}$ ,  $NO_3^-$ , and  $NH_4^+$ ) varied fairly consistently with that of  $PM_{2.5}$ , indicating fossil fuel combustions (e.g. coal combustion and traffic emissions) were the major sources of the severe air pollution in this study.

The temporal variations of trace elements in  $PM_{2.5}$  (Fig. S2) could further characterize the emission sources of pollution since they were mainly derived from primary emissions. Trace elements were categorized into two groups, i.e. mineral elements (Fig. S2a) and pollution elements (Fig. S2b–d). The two groups showed distinctly different temporal variations. The temporal variations of the mineral elements (i.e. Al, Ca, and Ti) varied quite inconsistently with that of  $PM_{2.5}$  and inorganic ions. During the cold fronts as discussed above, mineral elements presented higher concentrations and

Beijing 2013 extreme  
haze pollution

K. Huang et al.

Title Page

Abstract

Introduction

Conclusions

References

Tables

Figures

◀

▶

◀

▶

Back

Close

Full Screen / Esc

Printer-friendly Version

Interactive Discussion



the fraction of mineral aerosol in  $PM_{2.5}$  reached  $(35.2 \pm 14.2)\%$ . While during the high pollution episodes, the mineral elements showed lower concentrations conversely with a much lower mineral fraction of  $(6.3 \pm 4.9)\%$ . As for the pollution elements, their temporal variations showed similar patterns as that of  $PM_{2.5}$  and inorganic ions. As shown in Fig. S2b, arsenic (As) presented a concurrent variation with S and both showed peaks during the fog days. Since As and S were both good tracers for coal combustion, this corroborated that the severe pollution episode during the fog days was partly related to the enhanced coal combustion. Figure S2c and d show another two groups of pollution elements. Zn, Cu, and Cd could be regarded as the tracers for industrial emissions, and Ni, V, and Pb were mainly derived from the vehicle emission (Huang et al., 2012). These elements also showed significant enhancement during the fog days. Thus, it was likely that enhanced industrial and traffic emissions also contributed to this severe pollution episode.

### 3.4 Impact of relative humidity on aerosol chemistry

According to the discussions above, relative humidity (RH) played an important role in the evolution and transformation of aerosol species. Figure 6 shows the variation of aerosol components as a function of RH. Nonlinear regressions (exponential growth regression equation:  $y = a \times \exp(bx)$ ) were fitted for each species as indicated by the blue curves. Although the number of observation data was limited, all aerosol species still presented an explicit trend as the function of RH.  $SO_4^{2-}$ ,  $NO_3^-$ , and  $NH_4^+$  showed the most significant exponential relationship with RH. At relatively low RH (e.g. less than 50%), the increasing rates of these species were not so outstanding mainly due to that these species had not reached their deliquescence RH values. As RH increased, more prominent increases of aerosol species were evidently observed. At high RH, more amounts of pollutant precursors, such as  $SO_2$ ,  $NO_x$ , and  $NH_3$  could be adsorbed due to the increased liquid water content. On the other hand, the aqueous-phase processing due to high RH could also accelerate the transformation of  $SO_2$  and  $NO_x$  to acids via the oxidation pathways, such as the  $H_2O_2/O_3$  oxidation and metal catalysis (e.g.



reactions (Huang et al., 2006). Although the total organic aerosol was not measured in this study, the strong dependence of oxalate on RH suggested that the secondary organic aerosol (SOA) also played an important role in the haze formation (Zhang et al., 2013).  $\text{Cl}^-$  had a moderate increase of less than 2 folds during fog days. Other ions such as  $\text{F}^-$ ,  $\text{NO}_2^-$ ,  $\text{Na}^+$ ,  $\text{Mg}^{2+}$  and  $\text{Ca}^{2+}$  all showed negligible differences between the two periods.

### 3.5 Impact of fog processing on the aerosol acidity

As shown in Table 1, the ratio of  $\text{NH}_4^+$  in fog days vs. non-fog days was lower than that of  $\text{SO}_4^{2-}$  and  $\text{NO}_3^-$ . Since these three ions were the major species determining the acidity of aerosol, the aerosol under the circumstances of fog occurrences would become more acidic. Figure 7a plots the relationship between the equivalent concentrations ( $\mu\text{eq m}^{-3}$ ) of total anions and total cations grouped by the fog and non-fog days. Linear regression equations were fit for each group and the 1 : 1 dash line in Fig. 7a meant a neutralized ionic system without deficit or surplus of any hydrogen ions ( $\text{H}^+$ ). During the non-fog days, most of the observation data distributed around the 1 : 1 line. As the ionic concentrations increased, the scatters tended to lie above the 1 : 1 line, indicating more deficits of cations, i.e.  $\text{H}^+$ . Overall, the regression slope during the non-fog days was 1.3, indicating the aerosol was moderately acidic. While in the fog days, a much more elevated regression slope was found with the value of 2.4 (Fig. 7a), indicating considerable amounts of  $\text{H}^+$  existing in aerosol. Very tight correlations ( $R > 0.99$ ) were found for both fog days and non-fog days, indicating that the amount of  $\text{H}^+$  increased with the ionic strength, or in others words, with enhanced emissions. Figure s3 shows the temporal variations of the calculated  $\text{H}_{\text{Aer}}^+$  concentration and the ratio of  $\text{H}_{\text{Aer}}^+$  in the total inorganic ions (definition described in Sect. 2.4). During the non-fog days (1–9 January), five days out of total nine days showed that aerosols were completely neutralized. For the remaining four days,  $\text{H}_{\text{Aer}}^+$  averaged  $0.10 \mu\text{mol m}^{-3}$  and contributed about 7.5 % of the total ions, while during the fog days (10–15 January),

[Title Page](#)[Abstract](#)[Introduction](#)[Conclusions](#)[References](#)[Tables](#)[Figures](#)[◀](#)[▶](#)[◀](#)[▶](#)[Back](#)[Close](#)[Full Screen / Esc](#)[Printer-friendly Version](#)[Interactive Discussion](#)

the concentration of  $H_{Aer}^+$  was much more enhanced to an average of  $0.62 \mu\text{mol m}^{-3}$ , which contributed about 17.3% of the total ions.

To further investigate the speciation of sulfate and nitrate under the acidic environment, the relationship between  $H_{Aer}^+$  and the sum of  $\text{SO}_4^{2-}$  and  $\text{NO}_3^-$  (equivalent concentrations,  $\mu\text{eq m}^{-3}$ ) during the whole study period is plotted in Fig. 7b. Acidic and neutralized aerosols are distinguished by different colors. The horizontal dash line represented neutralized acids as the concentrations of  $H_{Aer}^+$  were equaled to zero, thus  $\text{SO}_4^{2-}$  and  $\text{NO}_3^-$  were in the form of  $(\text{NH}_4)_2\text{SO}_4$  and  $\text{NH}_4\text{NO}_3$ . The 1 : 1 dash line represented that  $\text{SO}_4^{2-}$  and  $\text{NO}_3^-$  were in the form of free acids, i.e.  $\text{H}_2\text{SO}_4$  and  $\text{HNO}_3$ . It is obvious that the concentrations of neutralized aerosols were much lower than those acidic aerosols as indicated in Fig. 7b. As for the acidic aerosol samples,  $H_{Aer}^+$  correlated very tightly with the sum of  $\text{SO}_4^{2-}$  and  $\text{NO}_3^-$  ( $R = 0.99$ ). Most importantly, the linear regression slope was around 0.6, much lower than the unity. This clearly indicated that  $\text{SO}_4^{2-}$  and  $\text{NO}_3^-$  were partially neutralized and partially in the form of free acids. For  $(\text{NH}_4)_2\text{SO}_4$  in the presence of free  $H^+$ , part of  $\text{SO}_4^{2-}$  would exist in the form of bisulfate, i.e.  $\text{NH}_4\text{HSO}_4$ . Thus, the acidic aerosol in this study should be a mixture of  $(\text{NH}_4)_2\text{SO}_4$ ,  $\text{NH}_4\text{NO}_3$ ,  $\text{NH}_4\text{HSO}_4$ ,  $\text{H}_2\text{SO}_4$  and  $\text{HNO}_3$ .

The E-AIM model described in Sect. 2.4 gave a solution of the state of an ionic system, generating liquid water content and dissolved ions in the aqueous phase present at equilibrium. Specifically, the concentrations of free hydrogen ( $H_{Aq}^+$ ) and bisulfate ( $\text{HSO}_4^-$ ) were simulated. Thus, the amount of  $\text{NH}_4\text{HSO}_4$  and free acids could be estimated. The equivalent concentration of  $\text{NH}_4\text{HSO}_4$ ,  $[\text{NH}_4\text{HSO}_4]_{\text{eq}}$ , equaled to  $[\text{HSO}_4^-]_{\text{AIM}}$ . Here and hereinafter the subscript AIM denotes the equivalent concentrations simulated by the E-AIM model. Since it was difficult to quantify the relative concentrations of the single  $\text{H}_2\text{SO}_4$  and  $\text{HNO}_3$ , we calculated their total equivalent concentration as  $[\text{Free acids}]_{\text{eq}} = [H_{Aq}^+]_{\text{AIM}}$ . The fraction of  $(\text{NH}_4)_2\text{SO}_4$  and  $\text{NH}_4\text{NO}_3$  in the neutralized acids could vary, thus we also grouped them together as total neutralized ammonium salts (TNAS). In regard of the acidic aerosol with deficit of  $\text{NH}_4^+$ , the equivalent

Title Page

Abstract

Introduction

Conclusions

References

Tables

Figures

◀

▶

◀

▶

Back

Close

Full Screen / Esc

Printer-friendly Version

Interactive Discussion



Beijing 2013 extreme  
haze pollution

K. Huang et al.

Title Page

Abstract

Introduction

Conclusions

References

Tables

Figures

◀

▶

◀

▶

Back

Close

Full Screen / Esc

Printer-friendly Version

Interactive Discussion



concentration of TNAS was calculated to be:  $[\text{TNAS}]_{\text{eq}} = [\text{NH}_4^+]_{\text{eq}} - [\text{HSO}_4^-]_{\text{AIM}}$ . During the fog days from 10–15 January, the average ratio of  $\text{H}_{\text{Aq}}^+/\text{H}_{\text{Aer}}^+$  and  $[\text{HSO}_4^-]/[\text{SO}_4^{2-}]$  reached 0.56 and 0.52, respectively, indicating a strong lack of neutralization. Figure 8 shows the fractional contribution of free acids,  $\text{NH}_4\text{HSO}_4$  and TNAS in the total acids with focus on the fog days from 10–15 January. Free acids contributed the most ( $> 40\%$ ) to the total acids on 12 January, which was the most polluted day in this study (see Figs. 4 and 5). Accordingly, the amount of completely neutralized acids contributed least of about 38%. This was consistent with previous study in Pittsburg that higher  $\text{SO}_4^{2-}$  events were generally less neutralized than those of lower concentrations (Zhang et al., 2007b). As for January 10, 11, and 13, their concentrations of  $\text{SO}_4^{2-}$ ,  $\text{NO}_3^-$ , and  $\text{NH}_4^+$  were in the similar level (Fig. 5). Figure 8 shows that the fractional contributions of free acids,  $\text{NH}_4\text{HSO}_4$ , and TNAS on these three days were also in the similar level. Compared to the first four fog days, the contributions of free acids to the total acids were much lower of  $\sim 20\%$  and  $10\%$  on 14 and 15 January, respectively. 60–80% of the acids were completely neutralized with a small portion of  $\text{NH}_4\text{HSO}_4$  of about 15%. The neutralization factor defined as the equivalent ratio of  $\text{NH}_4^+$  vs.  $[\text{SO}_4^{2-} + \text{NO}_3^-]$  was only  $0.56 \pm 0.05$  during the first four fog days. On the last two fog days, the  $\text{NH}_4^+ / [\text{SO}_4^{2-} + \text{NO}_3^-]$  ratio increased to  $0.76 \pm 0.09$ . The significant decreases of  $\text{SO}_4^{2-}$  and  $\text{NO}_3^-$  concentrations on the last two days (Fig. 5) should be the major cause for the lower acidities of aerosol. Figure 8 also shows the daily liquid water content (LWC) and the particle in situ pH value ( $\text{pH}_{\text{is}}$ ) simulated by the E-AIM model. LWC is a parameter dependent on relative humidity and the mass of water soluble aerosol (Xue et al., 2011). LWC reached the highest of  $22.75 \mu\text{mol m}^{-3}$  on 12 January. That's because, on one hand, RH reached the highest of 83.1% during the whole study; On the other hand, water soluble ions also reached the highest concentration. 10, 11, and 13 January were the days when the concentrations of water soluble ions were similar as discussed above. Higher LWC on 13 January was attributed to its higher RH of about 80% compared to the other two days. LWC showed the lowest values on 14 and

## Beijing 2013 extreme haze pollution

K. Huang et al.

Title Page

Abstract

Introduction

Conclusions

References

Tables

Figures

◀

▶

◀

▶

Back

Close

Full Screen / Esc

Printer-friendly Version

Interactive Discussion



15 January. Although RH was still high around 80 %, the relatively low concentrations of the water soluble ions on these two days were the major cause of the lower LWC associated with the particles. The daily variation of  $\text{pH}_{\text{is}}$  did not coincide with either the total concentrations of water soluble ions or the fractional contribution of free acids in the total acids.  $\text{pH}_{\text{is}}$  was the result of the combined effects of LWC and the magnitudes of free acids. As shown in Figs. S3 and 8,  $\text{H}_{\text{Aer}}^+$  and the contribution of free acids in the total acids were both the highest on 12 January. However, its  $\text{pH}_{\text{is}}$  was only moderate. This could be explained by the strong dilution effect resulting from the high LWC.  $\text{pH}_{\text{is}}$  showed the lowest values on the first two fog days. Although their free acids were only 40 % of that on 12 January, LWCs were even lower of about 30 %. Thus, the more significant reduction of LWC than the concentration of free acids resulted in even lower values of  $\text{pH}_{\text{is}}$ . The last two fog days (14–15 January) showed the highest  $\text{pH}_{\text{is}}$  values. Relatively low  $\text{H}_{\text{Aq}}^+$  concentrations were the major cause. Overall, the  $\text{pH}_{\text{is}}$  values during this severe pollution episode ranged from  $-0.78$  to  $0.14$ . It was within the ranges from previous studies in Beijing, Shanghai, Lanzhou (Pathak et al., 2009), and Hong Kong (Xue et al., 2011). However, the average concentration of in-situ aerosol acidity  $\text{H}_{\text{Aq}}^+$  reached  $369 \pm 296 \mu\text{mol m}^{-3}$ , about 1.6 times of a rural mountainous site in Beijing during summer with humid and cloudy weather (Pathak et al., 2009), 12 times of another site in Beijing during spring (He et al., 2012), 4 times of Shanghai and Hong Kong (Pathak et al., 2009; Xue et al., 2011), and 15 times of Guangzhou (Pathak et al., 2009). The extremely high acidity in aerosol during this study should be due to that, enhanced anthropogenic emissions during the winter heating season yielded significant amounts of acid precursors such as  $\text{SO}_2$  and  $\text{NO}_x$ . Under the fog processing, a considerable fraction of these precursors was transformed to strong acids in aerosol as found in this study. However, at the same time, the  $\text{NH}_3$  emission was not enough for neutralizing all the acids. As illustrated by Wang et al. (2011), most areas of the North China Plain were in the  $\text{NH}_3$ -poor regime during winter. Since agriculture activities dominated the  $\text{NH}_3$  emission, the less agriculture intensity during the cold season resulted in the unbalance of alkaline and acidic precursors. The strong acidity in aerosol not only affected

**Beijing 2013 extreme haze pollution**

K. Huang et al.

Title Page

Abstract

Introduction

Conclusions

References

Tables

Figures

◀

▶

◀

▶

Back

Close

Full Screen / Esc

Printer-friendly Version

Interactive Discussion



the acid-catalyzed particle-phase reactions but also may cause adverse impacts on ecosystem through wet deposition. Two model simulation studies both showed significant underestimation of particle mass concentrations during this fog episode. Using the WRF/NAQPMS modeling system (Wang et al., 2014b),  $PM_{2.5}$  concentrations were significantly biased low in Shijiazhuang ( $\sim 260$  km southwest to Beijing) and Beijing during 10–13 January. Coarse model resolution, emission uncertainties, and the two-way feedback effect were ascribed to this model under-prediction. Another modeling study using the MM5/CMAQ system (Wang et al., 2013) also found similar problems that the modeled sulfate and nitrate concentrations were far less than the observations during 11–15 January. Based on this study, we assume the possible causes of model under-prediction as follows: (1) the physical process of fog formation was not explicitly represented in the meteorology model (2) aqueous-phase reaction of secondary inorganic aerosol formation in the chemical transport model was not treated well in the fog events due to possible reasons such as uptake coefficient of gas precursors, reaction rates and etc. This study provides observational evidence of the importance of fog processing on the formation of haze in China and also constrains for future model simulations.

#### 4 Conclusions

Starting from January 2013, China released its  $PM_{2.5}$  data of major cities in China at the very first time. However, a large-scale haze occurred right after this act. Northern China experienced the severest haze with monthly (January 2013) average  $PM_{2.5}$ ,  $SO_2$ , and  $NO_2$  concentrations exceeding 225, 200, and  $80 \mu g m^{-3}$ , respectively. The regions with high  $SO_2$  concentrations and high  $SO_2/NO_2$  ratios ( $> 1.0$ ) mainly located in the north, suggesting the great impact from winter heating. Surface  $PM_{10}$  mean concentration in Beijing during January 2013 reached record high (only slightly lower than 2006) based on a historical dataset from 2003–2013. In addition, the largest daily fluctuation occurred in 2013, indicating more occurrences of extreme pollution events. However,

## Beijing 2013 extreme haze pollution

K. Huang et al.

Title Page

Abstract

Introduction

Conclusions

References

Tables

Figures

◀

▶

◀

▶

Back

Close

Full Screen / Esc

Printer-friendly Version

Interactive Discussion



AOD during January 2013 was 40 % lower than that of 2006, suggesting the impact from the changed meteorology. Compared to the historical climatology (2007–2012), the meteorological conditions in January 2013 were especially favorable for the formation of haze, such as higher humidity (with high frequency of fog occurrence), lower temperature, lower PBL height, lower wind speed and etc. Relative humidity was found most related to the decreased visibility. Based on a half month field campaign conducted in Beijing,  $PM_{2.5}$  reached extremely high concentrations of  $299.2 \pm 79.1 \mu g m^{-3}$  with extremely low visibility of  $0.92 \pm 0.82$  km during a continuous fog episode. Under the circumstance of long – lasting fog, AOD obviously increased but associated with a decrease of Angstrom exponent. The fog processing on increasing the size of aerosol residual mode was investigated to be responsible for this. Major aerosol chemical species such as  $SO_4^{2-}$ ,  $NO_3^-$ ,  $NH_4^+$ ,  $Cl^-$ ,  $K^+$ , and  $C_2O_4^{2-}$  presented an explicit exponential relationship with relative humidity, suggesting the significant impact of aerosol hygroscopicity on the visibility impairment. Fog processing was found to be the major pathway of extremely high yields of secondary inorganic aerosol.  $SO_4^{2-}$  increased most about 5 folds in the fog days compared to the non-fog days.  $NO_3^-$  and  $NH_4^+$  both increased about 3 folds. At the same time, ammonia was not enough to neutralize all the acids, thus aerosol in the fog days was found much more acidic than in the non-fog days. The concentrations of  $H^+$  increased linearly with the sum of  $SO_4^{2-}$  and  $NO_3^-$ . The E-AIM model simulated that bisulfate ( $HSO_4^{2-}$ ) accounted for an average of 52 % in total sulfate and free hydrogen ion ( $H_{Aq}^+$ ) accounted for an average of 27 % in the total acids. The in situ aerosol pH ranged from  $-0.78$  to  $0.14$  during fog days. Enhanced coal combustion during the winter heating season along with traffic and industrial emissions were the major sources for this severe haze.

Supplementary material related to this article is available online at <http://www.atmos-chem-phys-discuss.net/14/7517/2014/acpd-14-7517-2014-supplement.pdf>.

*Acknowledgements.* This work was supported by National Natural Science Foundation of China (Grant nos. 21277030, 41128005 (fund for collaboration with overseas scholars)) and Beijing Natural Science Fund (Grant no. 8112008). We thank for the permission of using the E-AIM models (<http://www.aim.env.uea.ac.uk/aim/aim.php>) and the principal investigators of the AERONET Beijing site for establishing and maintaining this site. We also thank NOAA's National Climate Data Center and the Ministry of Environment Protection of China for access to their data.

## References

- Chow, J. C., Bachmann, J. D., Wierman, S. S. G., Mathai, C. V., Malm, W. C., White, W. H., Mueller, P. K., Kumar, N., and Watson, J. G.: Visibility: science and regulation – discussion, *J. Air Waste Manage.*, 52, 973–999, 2002.
- Clean-Air-Asia: Beijing's Air Pollution Episode (January 2013), available at: <http://cleanairinitiative.org/portal/node/11599> (last access: 24 January 2014), 2013.
- Clegg, S. L., Brimblecombe, P., and Wexler, A. S.: Thermodynamic model of the system  $\text{H}^+ - \text{NH}_4^+ - \text{SO}_4^{2-} - \text{NO}_3^- - \text{H}_2\text{O}$  at tropospheric temperatures, *J. Phys. Chem. A*, 102, 2137–2154, doi:10.1021/Jp973042r, 1998.
- Dubovik, O. and King, M. D.: A flexible inversion algorithm for retrieval of aerosol optical properties from Sun and sky radiance measurements, *J. Geophys. Res.-Atmos.*, 105, 20673–20696, 2000.
- Eck, T. F., Holben, B. N., Reid, J. S., Giles, D. M., Rivas, M. A., Singh, R. P., Tripathi, S. N., Bruegge, C. J., Platnick, S., Arnold, G. T., Krotkov, N. A., Carn, S. A., Sinyuk, A., Dubovik, O., Arola, A., Schafer, J. S., Artaxo, P., Smirnov, A., Chen, H., and Goloub, P.: Fog- and cloud-induced aerosol modification observed by the Aerosol Robotic Network (AERONET), *J. Geophys. Res.-Atmos.*, 117, D07206, doi:10.1029/2011jd016839, 2012.
- Friese, E. and Ebel, A.: Temperature dependent thermodynamic model of the system  $\text{H}^+ - \text{NH}_4^+ - \text{Na}^+ - \text{SO}_4^{2-} - \text{NO}_3^- - \text{Cl}^- - \text{H}_2\text{O}$ , *J. Phys. Chem. A*, 114, 11595–11631, doi:10.1021/Jp101041j, 2010.
- Gao, Y., Liu, X., Zhao, C., and Zhang, M.: Emission controls versus meteorological conditions in determining aerosol concentrations in Beijing during the 2008 Olympic Games, *Atmos. Chem. Phys.*, 11, 12437–12451, doi:10.5194/acp-11-12437-2011, 2011.

Title Page

Abstract

Introduction

Conclusions

References

Tables

Figures

◀

▶

◀

▶

Back

Close

Full Screen / Esc

Printer-friendly Version

Interactive Discussion



**Beijing 2013 extreme  
haze pollution**

K. Huang et al.

Title Page

Abstract

Introduction

Conclusions

References

Tables

Figures

◀

▶

◀

▶

Back

Close

Full Screen / Esc

Printer-friendly Version

Interactive Discussion



He, K., Zhao, Q., Ma, Y., Duan, F., Yang, F., Shi, Z., and Chen, G.: Spatial and seasonal variability of PM<sub>2.5</sub> acidity at two Chinese megacities: insights into the formation of secondary inorganic aerosols, *Atmos. Chem. Phys.*, 12, 1377–1395, doi:10.5194/acp-12-1377-2012, 2012.

5 Holben, B. N., Eck, T. F., Slutsker, I., Tanre, D., Buis, J. P., Setzer, A., Vermote, E., Reagan, J. A., Kaufman, Y. J., Nakajima, T., Lavenu, F., Jankowiak, I., and Smirnov, A.: AERONET – a federated instrument network and data archive for aerosol characterization, *Remote Sens. Environ.*, 66, 1–16, 1998.

10 Huang, K., Zhuang, G. S., Li, J. A., Wang, Q. Z., Sun, Y. L., Lin, Y. F., and Fu, J. S.: Mixing of Asian dust with pollution aerosol and the transformation of aerosol components during the dust storm over China in spring 2007, *J. Geophys. Res.-Atmos.*, 115, D00k13, doi:10.1029/2009jd013145, 2010a.

Huang, K., Zhuang, G. S., Lin, Y. F., Li, J. A., Sun, Y. L., Zhang, W. J., and Fu, J. S.: Relation between optical and chemical properties of dust aerosol over Beijing, China, *J. Geophys. Res.-Atmos.*, 115, D00k16, doi:10.1029/2009jd013212, 2010b.

15 Huang, K., Zhuang, G., Lin, Y., Wang, Q., Fu, J. S., Zhang, R., Li, J., Deng, C., and Fu, Q.: Impact of anthropogenic emission on air quality over a megacity – revealed from an intensive atmospheric campaign during the Chinese Spring Festival, *Atmos. Chem. Phys.*, 12, 11631–11645, doi:10.5194/acp-12-11631-2012, 2012.

20 Huang, X. F., Yu, J. Z., He, L. Y., and Yuan, Z. B.: Water-soluble organic carbon and oxalate in aerosols at a coastal urban site in China: Size distribution characteristics, sources, and formation mechanisms, *J. Geophys. Res.-Atmos.*, 111, D22212, doi:10.1029/2006jd007408, 2006.

25 Itahashi, S., Uno, I., Yumimoto, K., Irie, H., Osada, K., Ogata, K., Fukushima, H., Wang, Z., and Ohara, T.: Interannual variation in the fine-mode MODIS aerosol optical depth and its relationship to the changes in sulfur dioxide emissions in China between 2000 and 2010, *Atmos. Chem. Phys.*, 12, 2631–2640, doi:10.5194/acp-12-2631-2012, 2012.

Jacobson, M. Z.: Development and application of a new air pollution modeling system, 2. Aerosol module structure and design, *Atmos. Environ.*, 31, 131–144, doi:10.1016/1352-2310(96)00202-6, 1997.

30 Li, J. J., Wang, G. H., Wang, X. M., Cao, J. J., Sun, T., Cheng, C. L., Meng, J. J., Hu, T. F., and Liu, S. X.: Abundance, composition and source of atmospheric PM<sub>2.5</sub> at a remote site in the Tibetan Plateau, China, *Tellus B*, 65, 20281, doi:10.3402/Tellusb.V65i0.20281, 2013.

**Beijing 2013 extreme  
haze pollution**

K. Huang et al.

Title Page

Abstract

Introduction

Conclusions

References

Tables

Figures

◀

▶

◀

▶

Back

Close

Full Screen / Esc

Printer-friendly Version

Interactive Discussion



Lu, A. G. and Hu, M.: Spatial and temporal variation of relative humidity of China in the past half century, *Software Engineering and Knowledge Engineering: Theory and Practice Advances in Intelligent and Soft Computing*, 162, 235–239, 2012.

Li, Z., Eck, T., Zhang, Y., Zhang, Y., Li, D., Li, L., Xu, H., Hou, W., Lv, Y., Goloub, P., and Gu, X.: Observations of residual submicron fine aerosol particles related to cloud and fog processing during a major pollution event in Beijing, *Atmos. Environ.*, 86, 187–192, 2014.

Ma, J. Z., Chen, Y., Wang, W., Yan, P., Liu, H. J., Yang, S. Y., Hu, Z. J., and Lelieveld, J.: Strong air pollution causes widespread haze-clouds over China, *J. Geophys. Res.-Atmos.*, 115, D18204, doi:10.1029/2009jd013065, 2010.

Pathak, R. K., Yao, X. H., Lau, A. K. H., and Chan, C. K.: Acidity and concentrations of ionic species of  $PM_{2.5}$  in Hong Kong, *Atmos. Environ.*, 37, 1113–1124, doi:10.1016/S1352-2310(02)00958-5, 2003.

Pathak, R. K., Louie, P. K. K., and Chan, C. K.: Characteristics of aerosol acidity in Hong kong, *Atmos. Environ.*, 38, 2965–2974, doi:10.1016/j.atmosenv.2004.02.044, 2004.

Pathak, R. K., Wu, W. S., and Wang, T.: Summertime  $PM_{2.5}$  ionic species in four major cities of China: nitrate formation in an ammonia-deficient atmosphere, *Atmos. Chem. Phys.*, 9, 1711–1722, doi:10.5194/acp-9-1711-2009, 2009.

Ramanathan, V., Li, F., Ramana, M. V., Praveen, P. S., Kim, D., Corrigan, C. E., Nguyen, H., Stone, E. A., Schauer, J. J., Carmichael, G. R., Adhikary, B., and Yoon, S. C.: Atmospheric brown clouds: hemispherical and regional variations in long-range transport, absorption, and radiative forcing, *J. Geophys. Res.-Atmos.*, 112, D22s21, doi:10.1029/2006jd008124, 2007.

Seinfeld, J. H. and Pandis, S. N.: *Atmospheric Chemistry and Physics: From Air Pollution to Climate Change*, Wiley, John & Sons, Incorporated, New York, 1203 pp., 2006.

Sun, Y. L., Zhuang, G. S., Tang, A. H., Wang, Y., and An, Z. S.: Chemical characteristics of  $PM_{2.5}$  and  $PM_{10}$  in haze-fog episodes in Beijing, *Environ. Sci. Technol.*, 40, 3148–3155, doi:10.1021/Es051533g, 2006.

Sun, Y. L., Wang, Z. F., Fu, P. Q., Yang, T., Jiang, Q., Dong, H. B., Li, J., and Jia, J. J.: Aerosol composition, sources and processes during wintertime in Beijing, China, *Atmos. Chem. Phys.*, 13, 4577–4592, doi:10.5194/acp-13-4577-2013, 2013a.

Sun, Z. Q., Mu, Y. J., Liu, Y. J., and Shao, L. Y.: A comparison study on airborne particles during haze days and non-haze days in Beijing, *Sci. Total Environ.*, 456, 1–8, doi:10.1016/j.scitotenv.2013.03.006, 2013b.

Beijing 2013 extreme  
haze pollution

K. Huang et al.

Title Page

Abstract

Introduction

Conclusions

References

Tables

Figures

◀

▶

◀

▶

Back

Close

Full Screen / Esc

Printer-friendly Version

Interactive Discussion



Tao, M. H., Chen, L. F., Su, L., and Tao, J. H.: Satellite observation of regional haze pollution over the North China Plain, *J. Geophys. Res.-Atmos.*, 117, D12203, doi:10.1029/2012jd017915, 2012.

van Donkelaar, A., Martin, R. V., Brauer, M., Kahn, R., Levy, R., Verduzco, C., and Villeneuve, P. J.: Global estimates of ambient fine particulate matter concentrations from satellite-based aerosol optical depth: development and application, *Environ. Health Persp.*, 118, 847–855, doi:10.1289/Ehp.0901623, 2010.

Wang, L. T., Wei, Z., Yang, J., Zhang, Y., Zhang, F. F., Su, J., Meng, C. C., and Zhang, Q.: The 2013 severe haze over the southern Hebei, China: model evaluation, source apportionment, and policy implications, *Atmos. Chem. Phys. Discuss.*, 13, 28395–28451, doi:10.5194/acpd-13-28395-2013, 2013.

Wang, S. X., Xing, J., Jang, C. R., Zhu, Y., Fu, J. S., and Hao, J. M.: Impact assessment of ammonia emissions on inorganic aerosols in east china using response surface modeling technique, *Environ. Sci. Technol.*, 45, 9293–9300, doi:10.1021/Es2022347, 2011.

Wang, Y., Zhuang, G. S., Tang, A. H., Yuan, H., Sun, Y. L., Chen, S. A., and Zheng, A. H.: The ion chemistry and the source of PM<sub>2.5</sub> aerosol in Beijing, *Atmos. Environ.*, 39, 3771–3784, doi:10.1016/j.atmosenv.2005.03.013, 2005.

Wang, Y., L. Yao, I. Wang, Z. Liu, D. Ji, G. Tang, J. Zhang, Y. Sun, B. Hu, and J. Xin: Mechanism for the formation of the January 2013 heavy haze pollution episode over central and eastern China, *Sci. China Earth Sci.*, 57, 14–25, doi:10.1007/s11430-013-4773-4, 2014a.

Wang, Z. F., Li, J., Wang, Z., Yang, W. Y., Tang, X., Ge, B. Z., Yan, P. Z., Zhu, L. L., Chen, X. S., Chen, H. S., Wand, W., Li, J. J., Liu, B., Wang, X. Y., Wand, W., Zhao, Y. L., Lu, N., and Su, D. B.: Modeling study of regional severe hazes over mid-eastern China in January 2013 and its implications on pollution prevention and control, *Sci. China Earth Sci.*, 57, 3–13, doi:10.1007/s11430-013-4793-0, 2014b.

Wong, E.: On scale of 0 to 500, Beijing's air quality tops crazy bad at 755, *New York Times*, 12 January 2013, 2013.

Xue, J., Lau, A. K. H., and Yu, J. Z.: A study of acidity on PM<sub>2.5</sub> in Hong Kong using online ionic chemical composition measurements, *Atmos. Environ.*, 45, 7081–7088, doi:10.1016/j.atmosenv.2011.09.040, 2011.

Yuan, H., Wang, Y., and Zhuang, G. S.: Simultaneous determination of organic acids, methanesulfonic acid and inorganic anions in aerosol and precipitation samples by ion chromatography, *Journal of Instrumental Analysis*, 22, 11–44, 2003.

**Beijing 2013 extreme  
haze pollution**

K. Huang et al.

Title Page

Abstract

Introduction

Conclusions

References

Tables

Figures

◀

▶

◀

▶

Back

Close

Full Screen / Esc

Printer-friendly Version

Interactive Discussion



- Zhang, J. K., Sun, Y., Liu, Z. R., Ji, D. S., Hu, B., Liu, Q., and Wang, Y. S.: Characterization of submicron aerosols during a serious pollution month in Beijing (2013) using an aerodyne high-resolution aerosol mass spectrometer, *Atmos. Chem. Phys. Discuss.*, 13, 19009–19049, doi:10.5194/acpd-13-19009-2013, 2013.
- 5 Zhang, M. S., Song, Y., and Cai, X. H.: A health-based assessment of particulate air pollution in urban areas of Beijing in 2000–2004, *Sci. Total Environ.*, 376, 100–108, doi:10.1016/j.scitotenv.2007.01.085, 2007a.
- Zhang, Q., Jimenez, J. L., Worsnop, D. R., and Canagaratna, M.: A case study of urban particle acidity and its influence on secondary organic aerosol, *Environ. Sci. Technol.*, 41, 3213–3219, doi:10.1021/Es061812j, 2007b.
- 10 Zhang, R., Q. Li, and R. Zhang: Meteorological conditions for the persistent severe fog and haze event over eastern China in January 2013, *Sci. China Earth Sci.*, 57, 26–35, doi:10.1007/s11430-013-4774-3, 2014.
- Zhang, X. Y., J. Sun, Y. Wang, W. Li, Q. Zhang, W. Wang, J. Quan, G. Cao, J. Wang, Yang, Y., and Zhang, Y.: Factors contributing to haze and fog in China, *Chinese Sci. Bull.*, 58, 1178–1187, 2013 (in Chinese).
- 15 Zhao, X. J., Zhao, P. S., Xu, J., Meng, W., Pu, W. W., Dong, F., He, D., and Shi, Q. F.: Analysis of a winter regional haze event and its formation mechanism in the North China Plain, *Atmos. Chem. Phys.*, 13, 5685–5696, doi:10.5194/acp-13-5685-2013, 2013.
- 20 Zhuang, G. S., Guo, J. H., Yuan, H., and Zhao, C. Y.: The compositions, sources, and size distribution of the dust storm from China in spring of 2000 and its impact on the global environment, *Chinese Sci. Bull.*, 46, 895–901, 2001.

## Beijing 2013 extreme haze pollution

K. Huang et al.

Title Page

Abstract

Introduction

Conclusions

References

Tables

Figures

◀

▶

◀

▶

Back

Close

Full Screen / Esc

Printer-friendly Version

Interactive Discussion



**Table 1.** Mean value and standard deviation of major meteorological parameters and ionic species during Period I (4–9 January) and Period II (10–15 January), respectively. The ratios of the mean values of Period II vs. Period I for each parameter are shown in the last column.

	Period I (4–9 Jan)		Period II (10–15 Jan)		Ratio*
	Mean	S.D.	Mean	S.D.	
Temp (°C)	265.2	4.1	267.7	3.5	1.01
RH (%)	37.4	11.1	77.5	5.1	2.07
PBL (m)	264.3	179.7	234.2	109.9	0.89
WS (ms <sup>-1</sup> )	2.43	1.7	1.8	1.0	0.75
F <sup>-</sup>	0.19	0.12	0.22	0.10	1.17
Cl <sup>-</sup>	2.89	2.43	7.57	3.72	2.62
NO <sub>2</sub> <sup>-</sup>	0.10	0.11	0.11	0.06	1.15
NO <sub>3</sub> <sup>-</sup>	6.88	5.75	28.58	11.28	4.16
SO <sub>4</sub> <sup>2-</sup>	7.81	5.71	44.32	23.22	5.68
C <sub>2</sub> O <sub>4</sub> <sup>2-</sup>	0.15	0.08	0.54	0.24	3.74
Na <sup>+</sup>	0.57	0.22	0.95	0.45	1.67
NH <sub>4</sub> <sup>+</sup>	4.34	3.01	14.64	4.92	3.37
K <sup>+</sup>	0.81	0.80	4.15	2.11	5.14
Mg <sup>2+</sup>	0.23	0.02	0.23	0.00	0.98
Ca <sup>2+</sup>	0.51	0.17	0.44	0.27	0.86

\*The ratio of the mean values of Period II vs. Period I for each parameter.

## Beijing 2013 extreme haze pollution

K. Huang et al.

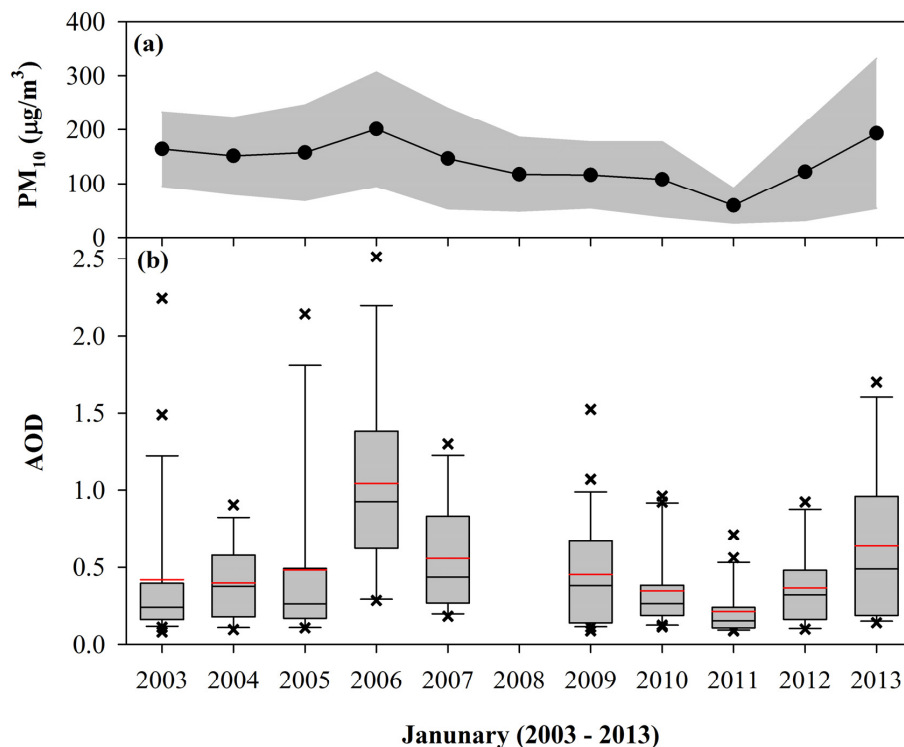


**Fig. 1.** Monthly average values of **(a)** AOD (Aerosol Optical Depth, Level 2.0 data from AERONET) and **(b)** surface  $PM_{10}$  concentrations over Beijing in each January during multi-years from 2003 to 2013. The shaded areas in Fig. 1a represent one standard deviation above and below the average values; The red and black lines inside the boxes represent the mean and median values; bottom and top of the boxes represent the 25 and 75 % limits, respectively; and bottom and top short lines represent the minimum and maximum values, respectively; black dots represent the outliers.

Beijing 2013 extreme  
haze pollution

K. Huang et al.

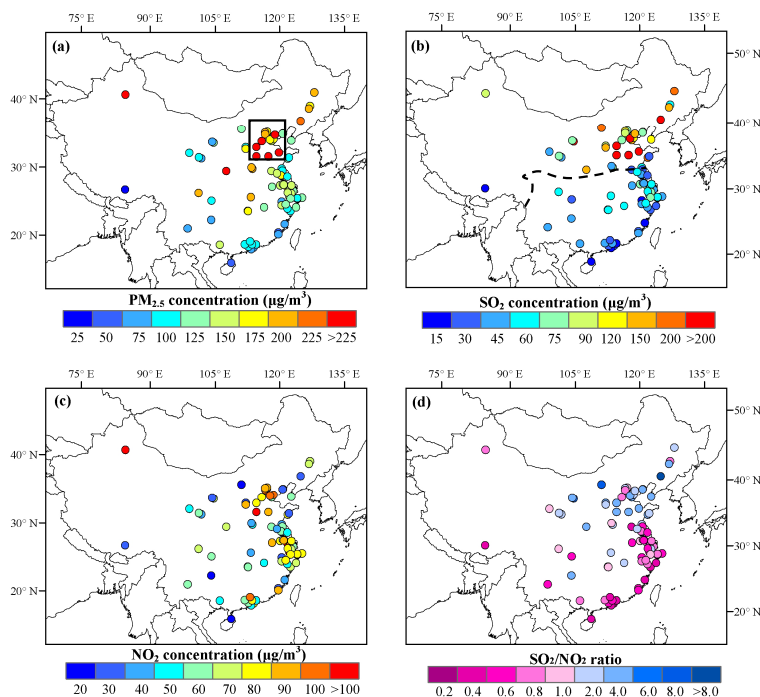


**Fig. 2.** The spatial distribution of mean concentrations of (a)  $\text{PM}_{2.5}$ , (b)  $\text{SO}_2$ , (c)  $\text{NO}_2$ , and (d) the  $\text{SO}_2/\text{NO}_2$  ratios at 74 Chinese cities during January 2013. The Beijing-Tianjin-Hebei region is highlighted by the black rectangle in Fig. 2a. The dashed line in Fig. 2b represents the heating supply line that separates the northern heating region from the non-heating region (source: <http://www.infzm.com/content/84193>, in Chinese).

Title Page

Abstract

Introduction

Conclusions

References

Tables

Figures

◀

▶

◀

▶

Back

Close

Full Screen / Esc

Printer-friendly Version

Interactive Discussion



## Beijing 2013 extreme haze pollution

K. Huang et al.

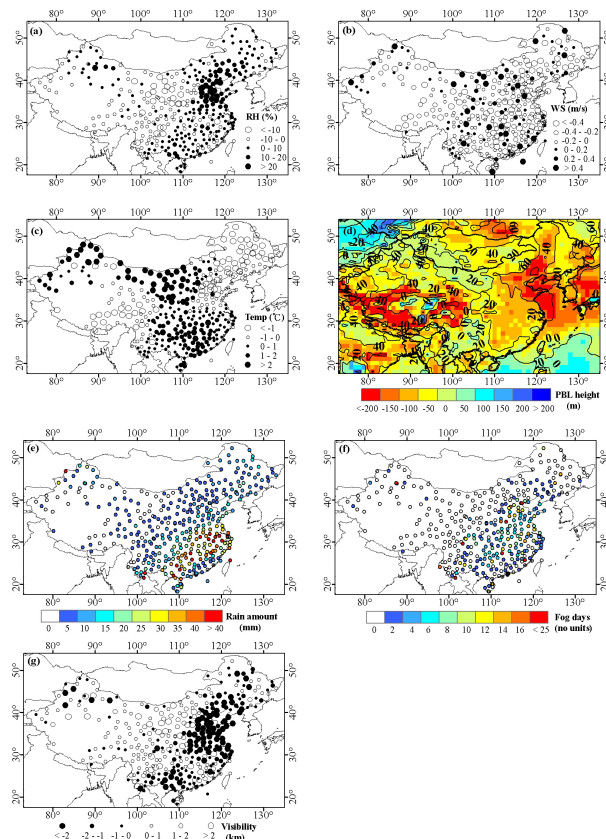


**Fig. 3.** The difference of **(a)** relative humidity, **(b)** wind speed, **(c)** temperature, **(d)** planetary boundary layer height (contour line represents the fraction of decreased PBL height in 2013 compared to previous years), and **(g)** visibility between January 2013 and the average values during the same period from 2007 to 2012. **(e)** The total precipitation amount and **(f)** total number of fog days in January 2013.

## Beijing 2013 extreme haze pollution

K. Huang et al.

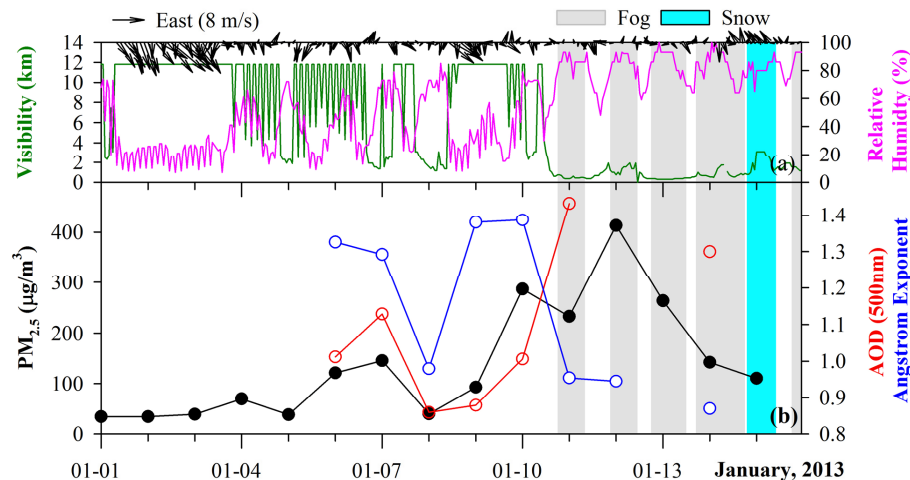


**Fig. 4.** (a) Hourly variations of relative humidity, visibility and wind vectors during 1–15 January 2013. (b) Daily variations of  $PM_{2.5}$  concentrations, AOD (500 nm) and Angstrom exponent (440–870 nm). The occurrences of fog and snow are highlighted by the gray and light blue bars in the figure.

Title Page

Abstract

Introduction

Conclusions

References

Tables

Figures

◀

▶

◀

▶

Back

Close

Full Screen / Esc

Printer-friendly Version

Interactive Discussion



Beijing 2013 extreme  
haze pollution

K. Huang et al.

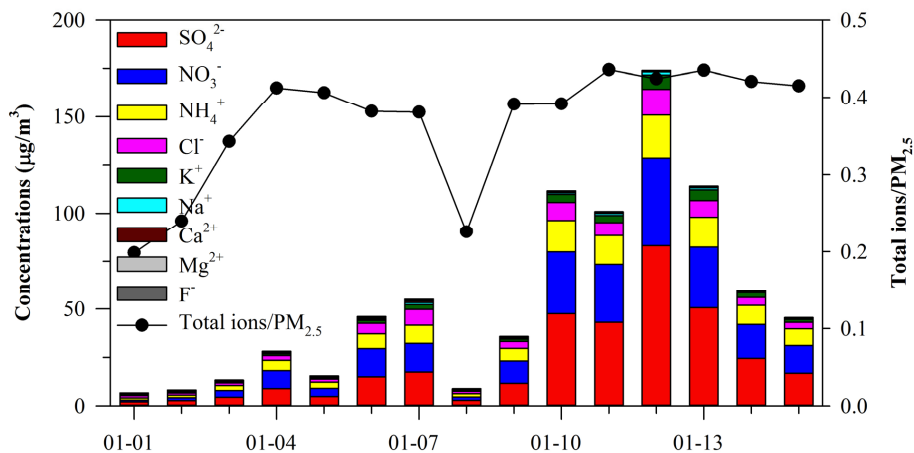


Fig. 5. Time-series of major aerosol inorganic species and the ratios of total ions in PM<sub>2.5</sub>.

Title Page

Abstract

Introduction

Conclusions

References

Tables

Figures

◀

▶

◀

▶

Back

Close

Full Screen / Esc

Printer-friendly Version

Interactive Discussion



## Beijing 2013 extreme haze pollution

K. Huang et al.

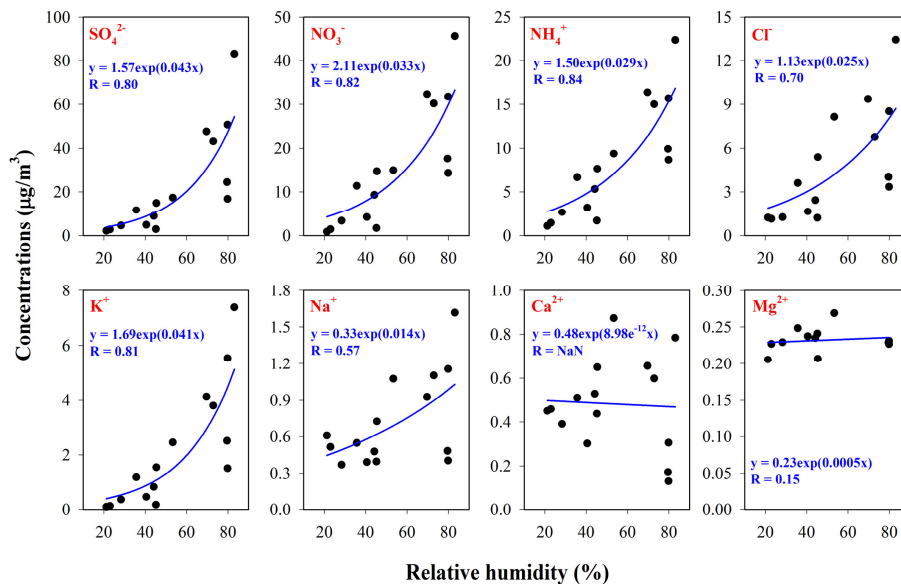


**Fig. 6.** The variations of the concentrations of major aerosol inorganic species as a function of relatively humidity. Exponential growth regression curves ( $y = a \times \exp(bx)$ ) are fitted as denoted by the blue lines. The regression equations with correlation coefficients ( $R$ ) are shown in the figure for each species.

Title Page

Abstract

Introduction

Conclusions

References

Tables

Figures

◀

▶

◀

▶

Back

Close

Full Screen / Esc

Printer-friendly Version

Interactive Discussion



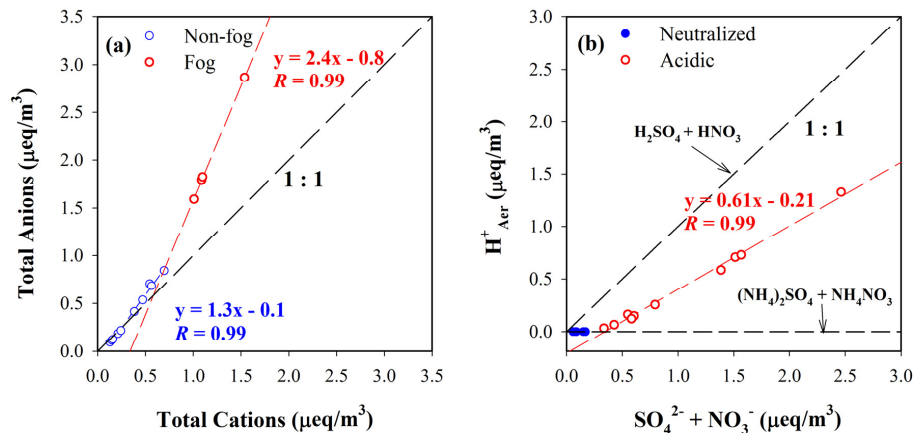


**Fig. 7.** (a) The linear relationship between the total anions and the total cations grouped by fog and non-fog days. Linear regression equation is fit for both groups. The 1 : 1 line represents the charge balanced ionic system. (b) The relationship between the calculated hydrogen ion ( $\text{H}^+_{\text{Aer}}$ ) and the sum of  $\text{SO}_4^{2-}$  and  $\text{NO}_3^-$  grouped by neutralized and acidic aerosols. Linear regression equation is fit for the acidic aerosol.

## Beijing 2013 extreme haze pollution

K. Huang et al.

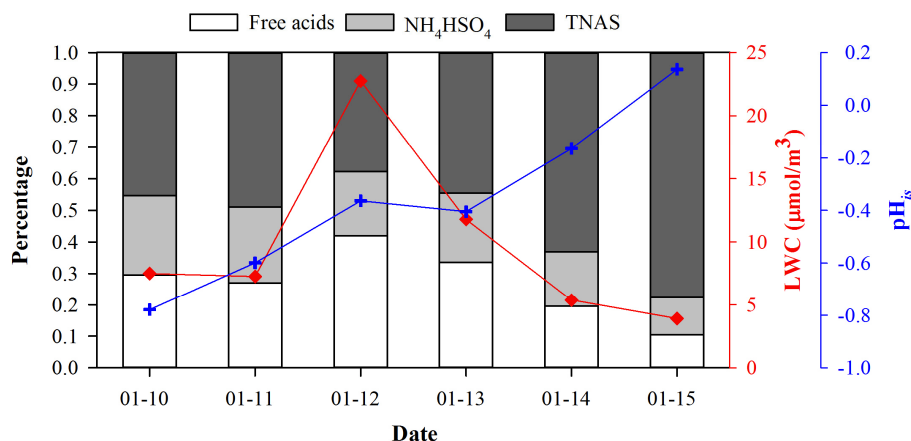


**Fig. 8.** Bars represent the fractional contribution of free acids,  $\text{NH}_4\text{HSO}_4$  and the total neutralized ammonium salts (TNAS) in the total acids during the fog days from 10–15 January. Lines represent the liquid water content (LWC) and the in situ pH value in aerosol ( $\text{pH}_{\text{is}}$ ) simulated by the E-AIM model.

Title Page

Abstract

Introduction

Conclusions

References

Tables

Figures

◀

▶

◀

▶

Back

Close

Full Screen / Esc

Printer-friendly Version

Interactive Discussion

